International Journal of Hydrogen Energy 130 (2025) 440–451

Contents lists available at ScienceDirect

International Journal of Hydrogen Energy

journal homepage: www.elsevier.com/locate/he

Hydrogen storage of Mg–3Zn–1Ca-0.5Mn industrial scale magnesium ring processed by hot upsetting and radial axial ring rolling

H. Vafaeenezhad [a,*], B. Nateq [a], M. Mahmoudi [b], M. Fesahat [b], Sh Azizpour [b]

[a] Department of Materials Science and Engineering, Faculty of Engineering, Ferdowsi University of Mashhad, Azadi Square, Mashhad, Iran
[b] School of Materials Science & Engineering, Iran University of Science and Technology, Narmak, Tehran, Iran

ARTICLE INFO

Handling Editor: Suleyman I. Allakhverdiev

Keywords:
ZX31 Mg alloy
Dynamic recrystallization
Upsetting
Ring rolling
Hydrogen storage

ABSTRACT

An industrial plastic deformation method involving large strain induction, known as ring rolling (RR), was applied after initial upsetting to produce an ultra-fine-grained Mg ring part with superior hydrogen storage capabilities at industrial scale. The microstructure evolution and hydrogen storage characteristics of the Mg–3Zn–1Ca-0.5Mn alloy (ZX31) were analyzed to establish a correlation between grain structure and hydrogen storage behavior. The enhanced hydrogen storage performance of the ring-rolled material was compared to the upset-only condition using Sievert testing. Results revealed that hydrogen absorption and desorption kinetics are governed by the level of plastic strain and the associated microstructure/substructure modifications induced during processing. Grain refinement achieved through hybrid hot upsetting-ring rolling promoted the formation of effective interfaces, leading to improved hydrogen uptake kinetics. Transmission electron microscopy (TEM) of the severely deformed samples showed the development of dislocation substructures, highlighting their critical role in controlling hydrogen storage performance. Finally, the relationship between hydrogen storage and release kinetics and the microstructure-substructure features was discussed.

1. Introduction

With growing concerns over reducing carbon emissions and adopting hydrogen as a clean, renewable energy source, the field of hydrogen storage has gathered significant research interest. Among various metal hydrides, magnesium hydride (MgH_2) has emerged as a promising solid-state hydrogen storage medium due to its relatively high storage capacity and cost-effective production [1–4]. However, the kinetics of hydrogen absorption and desorption in magnesium alloys with coarse grains are often suboptimal, posing challenges from both kinetic and thermodynamic perspectives [5].

In such cases, the onset of hydrogen absorption in magnesium is hindered by operational complexities and financial constraints arising from the simultaneous need for elevated temperatures and pressures in a safe environment [6]. Alternatively, utilizing ultrafine-grained or nanostructured magnesium alloys as hydrogen hosts offers significant advantages. These materials provide a higher density of preferred reaction sites, leading to enhanced hydrogen absorption and desorption kinetics.

Methods for achieving such structural refinement typically involve high-energy and large-strain approaches, which can be broadly categorized into powder metallurgy and bulk severe plastic deformation (SPD) techniques. For example, Nivedhidha et al. [7] incorporated multi-walled carbon nanotubes (MWCNTs) into Mg–Ti binary systems via high-energy ball milling. Their findings indicated concurrent increases in crystal size and dislocation density, together with a reduction in lattice strain, all of which influence the hydrogen storage properties of the alloy.

However, while powder metallurgy offers certain advantages, it also presents notable limitations, such as surface contamination, extended processing times, fire hazards, and health risks. Moreover, activation of magnesium alloy powders through mechanochemical techniques is often economically and practically unviable due to the risk of unwanted surface oxidation and potential explosion hazards, which interfere with hydrogen storage performance [8,9].

On the other hand, bulk metal deformation techniques that induce severe plastic strains have been considered effective methods for processing hydrogen storage materials. Asselli et al. [10] studied the hydrogen storage performance of severely deformed ZK60 alloys processed via equal-channel angular pressing (ECAP) and accumulative roll bonding (ARB), both in bulk and crushed forms, and investigated their microstructure and morphology. Similarly, Floriano et al. [11] explored

* Corresponding author. Department of Materials Science and Engineering, Engineering Faculty, Ferdowsi University of Mashhad, Azadi Square, Mashhad, Iran.
E-mail addresses: h_vafaeenezhad@alumni.iust.ac.ir, hvafaeinezhad@um.ac.ir (H. Vafaeenezhad).

https://doi.org/10.1016/j.ijhydene.2025.04.122
Received 28 January 2025; Received in revised form 22 March 2025; Accepted 7 April 2025
Available online 27 April 2025

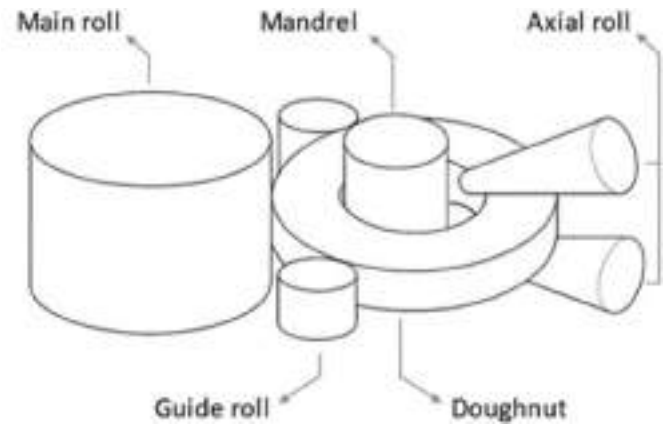

Fig. 1. Schematic illustration of a typical radial axial ring rolling machine.

the effect of rolling temperature and contamination on the hydrogen storage performance of the AZ91 alloy, correlating the extent of grain refinement to the alloy's absorption kinetics using in-depth SEM and XPS evaluations. Hout et al. [12] examined the hydrogen storage properties of AZ91 and MRI 153 magnesium alloys after cold rolling and forging, focusing on precipitation behavior and production methods, and compared the results with pure magnesium. However, these severe plastic deformation (SPD) methods cannot be considered practical for industrial applications as operational hydrogen storage solutions due to their batch processing nature and the size limitations of the final products. Wu et al. [13] studied the catalytic effect of in-situ formed Mg_2Ni and Mg_2Cu intermetallic compounds (IMC) in Mg–Cu_9A_{l4} composite considering the temperature-dependency and interface effect of hydrogen storage kinetics, thermodynamic properties, cyclic stability. Chen et al. constructed a Ni-reinforced 3D powder metallurgy carbon structure which was variegated with Mg to yield the Mg-based hydrogen storage system. Based on experimental and numerical simulation data, it was revealed that Ni deteriorates the Mg bonding to hydrogen, while carbon cell structure improves the effective hydrogen diffusion [14]. Aguilar et al. [15] produced an as-cast Mg-based hydrogen storage systems by adding Ni and Mishmetal which yield Mg_2Ni IMC within Mg matrix with superior chemical and oxidative resistance. Such alloying system can achieve high gravimetric storage performance and quick hydrogenation-dehydrogenation kinetics. [15]. Deng et al. [16] investigated the hydrogen storage properties of a series of Mg–Ti–V–Nb–Cr high entropy alloy and focused on the impact of Mg addition on the dehydrogenation temperature of developed alloy. Hu et al. [17] developed a rapidly solidified $Mg_{97}Ni_2Y_1$ alloy through melt-spinning which is with fiber with submicron-sized as reinforcement within α-Mg grains. The fine uniform amorphous microstructure formed can be considered as the main parameters for improved hydrogen storage [17]. Gorbel et al. [18] studied the catalytic effect of the CaNix IMC as the bed for extra inter-phase boundaries and crystal defects, which yield enhanced hydrogen diffusion throughout Mg-based solid solution matrix and lower its absorption and desorption temperatures. In contrast, the ring rolling process, which is classified as a forging method, has been widely used in the manufacturing of seamless metallic rings for various industries, including railways, gas turbine bearings, and jet engine components [13].

As illustrated in Fig. 1, a typical ring rolling mill consists of three main sets of rolls: radial rolls (mandrel and main roll) that control and set the radial thickness, axial rolls that maintain and limit the height of the forming ring, and guide rolls that preserve the round shape of the ring during the process while ensuring the required geometric tolerances [14]. This process offers several advantages, such as high production rates, consistent quality, superior surface finishes, and efficient use of materials and human resources [15].

Understanding the ring rolling process is challenging due to the complexity and diversity of parameters involved, which lead to inhomogeneous strain distributions throughout the deformation process [16]. Some of the critical factors influencing this process include the working temperature, friction effects, reduction ratios [17], initial material dimensions [13], idle roll feed rate [18] and the rotational speed of the main roll [19]. Improper configuration and control of these parameters can lead to defects in the final product, such as tilting geometries or the well-known fishtail defect [20]. Over the past decades, numerous experimental, numerical, and theoretical investigations have been conducted to analyze and optimize the ring rolling process for magnesium alloys [21–23].

Various process factors, such as rolling force, induced torque, temperature distribution, and damage probability, have been analyzed using physical models, the upper bound method, and integrated numerical–thermo-physical approaches [20,24,25]. Additionally, the material flow, plastic deformation behavior during forming, and the coupled influence of operational and metallurgical parameters have been investigated for both cold and hot ring rolling [16,24,26] Several studies have also focused on technological aspects and operational phenomena of this forming process, including side spread, pressure distribution, unwanted distortions in rings during post-process cooling, and even the crystallographic texture and plasticity of alloys in hot rolling [17,25–27].

This study focuses on the Mg–3Zn–1Ca-0.5Mn magnesium alloy and explores how hot upsetting followed by ring rolling influences its microstructural evolution and hydrogen storage performance. By applying these plastic deformation techniques, the primary aim is to improve the alloy's hydrogen absorption and desorption kinetics, which

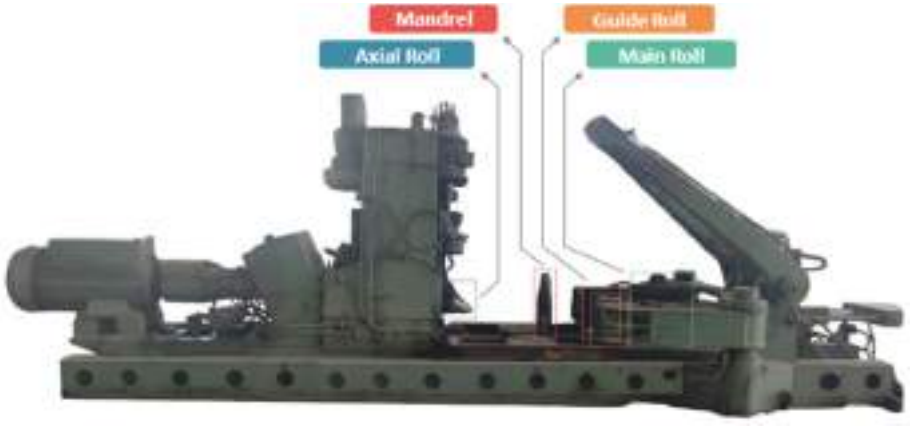

Fig. 2. The hot radial-axial ring rolling machine used in this research.

Fig. 3. (a) Ring rolled alloy in the final step of deformation, and (b) final product after cooling.

are critical for efficient hydrogen storage applications. The investigation examines the synergistic effects of upsetting and ring rolling on grain refinement, surface morphology, and the formation of crystallographic defects, all of which play critical roles in hydrogen diffusion and reaction kinetics. A comprehensive analysis links these microstructural modifications to the observed hydrogen storage behavior, providing insights into optimizing the alloy for practical use.

2. Experimental procedures

The starting material used in this study was ZX31 + 0.5Mn (Mg −3 wt. % Zn-1 wt. % Ca- 0.5 wt % Mn) supplied in the form of extruded bars. The extruded rods, with a diameter of 125 mm, were cut into billets of 100 mm length. These billets were initially upset using a 1000-ton hydraulic press operating at a constant ram speed of 2 mm/s at 400 °C. The upsetting process, carried out using solid upper and lower dies, imposed a strain of approximately 0.5 on the material.

Following the upsetting process, the Mg alloy billets were pierced in two passes at 400 °C and subsequently air-cooled. The resulting doughnut-shaped blanks were then subjected to final radial-axial ring rolling at 430 °C using a ring rolling mill (Wagner- Dortmund) located at BF Steel Company, Iran (Fig. 2). The seamless rings produced had an outer diameter (OD) of 250 mm, an inner diameter (ID) of 200 mm, and a height (H) of 120 mm. The tooling material for all deformation rolls in the ring rolling mill was 55NiCrMov7 quenched and tempered tool steel.

During the ring rolling process, the main roll actively rotated, while the idle roll rotated freely, driven solely by the contact force exerted through sliding friction. The idle roll fed outward and approached the main roll. Guide rolls and axial rolls were employed to prevent ring vibration and to eliminate fishtail defects along the axial path. Before the hot ring rolling (HRR) process, the ring blanks were preheated to 400 °C for 2 h, while the idle roll was preheated to 300 °C. The final dimensions of the seamless rings showed negligible changes in height, as shown in Fig. 3. The mandrel radial force was monitored to serve as a criterion for finite element method (FEM) validation. The main roll speed was set to 200 rpm, and the idle roll feed rate was maintained at 10 mm/s. The total strain imposed during the process was approximately 1.35, calculated based on the initial and final dimensions of the ring.

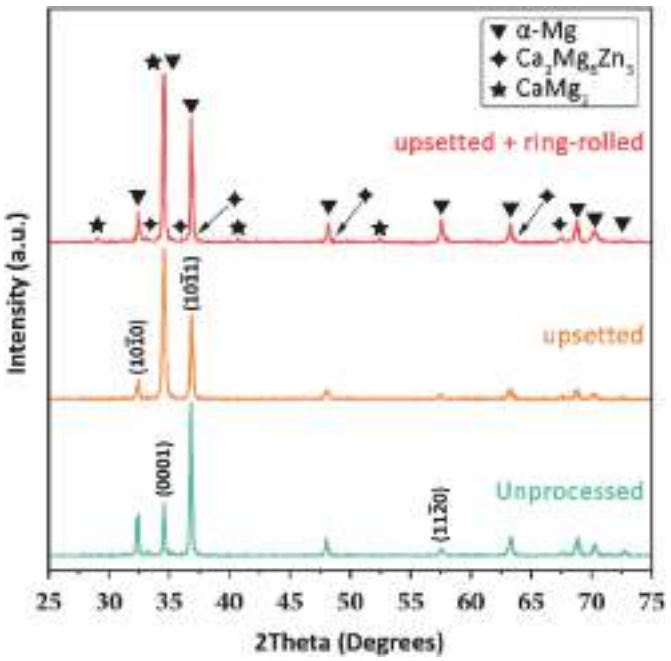

Fig. 4. The XRD patterns of ZX31 alloy in unprocessed state, after upsetting, and after upsetting followed by the ring-rolling process.

Before the hot ring rolling (HRR) process, the ring blanks were preheated to 400 °C for 2 h, while the idle roll was preheated to 300 °C. The final dimensions of the seamless rings showed negligible changes in height. The mandrel radial force was monitored to serve as a criterion for finite element method (FEM) validation.

For phase analysis and quantitative micro-state variable, X-ray diffraction (XRD) analysis was performed using a Bruker D8 Advance with Cu-K_α radiation. Microstructural evolution was studied using optical microscopy (OM), scanning electron microscopy (SEM), and transmission electron microscopy (TEM). SEM micrography was performed using a KYKY E8000 microscope, while TEM analysis was conducted using a ZEISS LEO912 microscope operating at 120 kV.

Hydrogen absorption and desorption kinetics were measured using an in-house Sieverts apparatus. Samples weighing approximately 100 mg were heated to 350 °C under vacuum, and hydrogen absorption and desorption were recorded under pressures of 2 MPa and 100 kPa of H_2, respectively.

3. Results and discussions

3.1. XRD pattern analysis

The XRD patterns of the ZX31 magnesium alloy for the un-processed, upsetted, and ring-rolled samples are shown in Fig. 4. The primary phase in all samples was indexed as a hexagonal close-packed (hcp) structure,

which is the crystal structure of magnesium. The relative intensity of the peaks associated with the hcp crystals provides insight into the dominant active deformation mechanisms in the material. For a typical predeformed material, the relative intensity ratio of the basal plane to the pyramidal plane is approximately 0.36 [10]. However, when the alloy is deformed under upsetting conditions, a preferred orientation develops along the basal plane of the hcp crystals (0001). Specifically, the intensity ratio of the basal plane to the pyramidal ($10\bar{1}$ 1) increases significantly to 1.8, which is substantially higher than the unbiased preference observed in raw magnesium material.

In contrast, under ring-rolling deformation conditions, the orientation along the pyramidal ($10\bar{1}$ 1) and prismatic (($10\bar{1}$ 0) and ($11\bar{2}$ 0)) planes becomes more pronounced, facilitating the material's ability to accommodate deformation. This indicates that in the 'upsetted + ring-rolled' sample, the basal plane remains dominant, while the pyramidal and prismatic planes are effectively contributing to accommodate the imposed strain. This texture-weakening phenomenon is commonly observed in Ca-containing Mg alloys subjected to hot deformation processes [28] and is associated with improved mechanical properties, including higher fracture elongation and reduced yield asymmetry [29].

Additionally, contraction twinning $\{101\ \bar{2}\}\langle 101\ \bar{1}\rangle$ is activated under tensile loading causing a 86.3° lattice reorientation and an extension along the c-axis of the twinned grains [1].

Fig. 4 also reveals the presence of low-intensity peaks corresponding to secondary phases along with the α(Mg) phase. Previous studies [28,30,31] have identified these secondary phases as the ternary intermetallic compound $Ca_2Mg_6Zn_3$ (JCPDS Card No. 12–0266) and $CaMg_2$ (COD ID: 1,536,923, Crystallography Open Database). The relatively weak diffraction peaks of these phases are relatively weak, commonly observed in similar research [30,32–34], can be attributed to the low alloying content and the limited volume fraction of this phase [33]. Furthermore, the structural and compositional characteristics of these phases are significantly influenced by the alloy's nominal composition, the Zn-to-Ca ratio, and its processing history [30].

3.2. Deformation and restoring mechanisms

The thermomechanical processing enhances hydrogen storage performance through three primary mechanisms. First, grain refinement plays a critical role by increasing the density of grain boundaries, which act as high-energy sites for hydrogen absorption and provide shorter diffusion paths for hydrogen atoms. Additionally, continuous dynamic recrystallization (CDRX) at high strain rates generates subgrain boundaries around newly formed grains, further facilitating hydrogen diffusion within the grains. This microstructural refinement ensures that hydrogen atoms can penetrate more efficiently, improving both absorption and desorption kinetics.

Second, mechanical twinning and anti-phase boundaries (APBs) introduced during deformation provide additional high-energy pathways for hydrogen diffusion. Although the energy of these features is lower than that of primary grain boundaries, they significantly contribute to enhancing hydrogen transport. Mechanical twins, in particular, create localized regions of high strain, which act as preferential sites for hydrogen absorption and desorption. Similarly, APBs formed during deformation provide additional interfaces that facilitate hydrogen diffusion, further optimizing the alloy's hydrogen storage performance.

Third, the strain distribution within the processed samples creates a gradient of high-energy sites, particularly in the central regions of the upsetted samples. This gradient enables hydrogen atoms to penetrate more effectively from the surface to the interior, ensuring uniform hydrogen distribution throughout the material. The combination of these mechanisms—grain refinement, twinning/APBs, and strain distribution—demonstrates that the thermomechanical processing parameters (temperature, strain rate, and deformation mechanisms) directly influence both microstructure and hydrogen storage performance.

Fig. 5. Optical micrograph of the as-received material.

3.2.1. Initial material characterization

The initial microstructure of the unprocessed material is shown in Fig. 5 The micrograph reveals equiaxed grains with an average size of 54 ± 7 µm. Variations in corrosion behavior during etching are likely due to differences in the crystallographic orientation of the grains relative to the sectioned surface. Mechanical twins are observed in some grains, often extending across their entire width.

3.2.2. Hot deformed structures

The microstructure of the sample after 50 % height reduction by upsetting is presented in Fig. 6a.

The deformation process has clearly induced dynamic recrystallization (DRX) near grain boundaries, where the compressive force is most intense. This resulted in the replacement of elongated grains with smaller, newly formed DRXed grains. The higher magnification in Fig. 6b reveals additional details, including ultrafine precipitates dispersed within the recrystallized grains and along grain boundaries. These precipitates are likely a result of dynamic precipitation during thermomechanical processing, as they align with the expected behavior of alloy systems undergoing severe plastic deformation [31]. Grains with distinct boundaries and evidence of significant refinement are also noticeable. The average DRXed grain size after upsetting is reduced to approximately 1 µm, although some elongated grains remain visible.

The ring-rolling process further refines the microstructure, as shown in Fig. 6c, with an enlarged view in Fig. 6d. The ring-rolling operation promotes additional DRX, as indicated by the emergence of very fine, uniformly distributed grains throughout the matrix. The microstructure in Fig. 6d highlights a further reduction in grain size, with a higher fraction of DRXed grains compared to the upset sample. The density of precipitates is also more prominent. These ultrafine precipitates are uniformly distributed, which suggests enhanced dynamic precipitation during the ring-rolling process.

A noteworthy feature observed in both processes is the formation of mechanical twins. These twins are visible in Fig. 6b and d, traversing entire grains in some cases. Twinning activity is particularly pronounced in the ring-rolled sample, as confirmed by the XRD patterns. The higher energy levels associated with twin boundaries, compared to the matrix grains, makes them effective pathways for hydrogen diffusion, much like grain boundaries.

Moreover, deformation-induced cracking in the bulk sample exposes rough surfaces. These rough interfaces increase the exposed surface area, further facilitating hydrogen sorption. Such structural characteristics play a crucial role in determining the material's performance

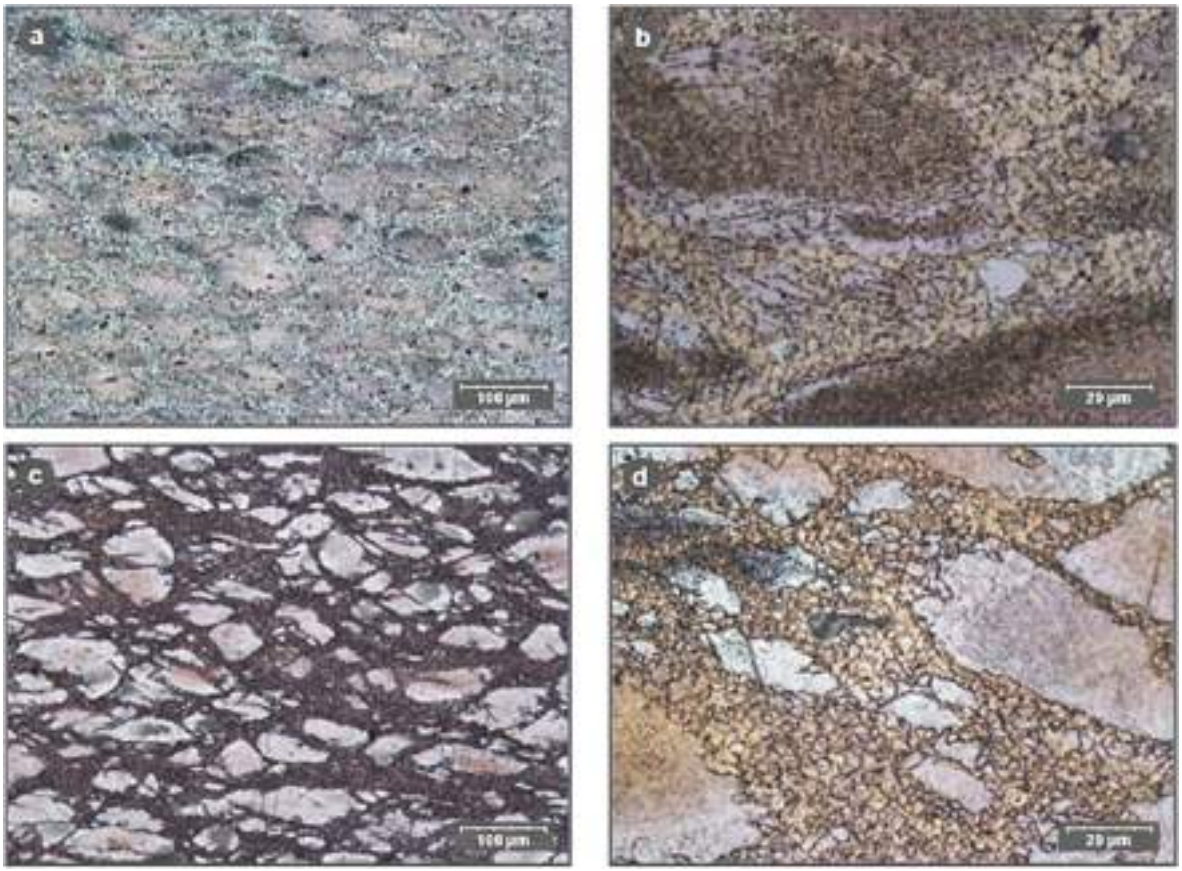

Fig. 6. Optical micrographs of the processed Mg–3Zn–1Ca-0.5Mn alloy showing microstructural evolution during thermomechanical processing; (a) overall microstructure after 50 % height reduction by upsetting; (b) higher magnification of (a) showing ultrafine precipitates within recrystallized grains and along grain boundaries (arrows); (c) microstructure after the ring-rolling process, highlighting further grain refinement and dynamic recrystallization; and (d) higher magnification of (c), revealing an increased density of ultrafine precipitates and deformation twins.

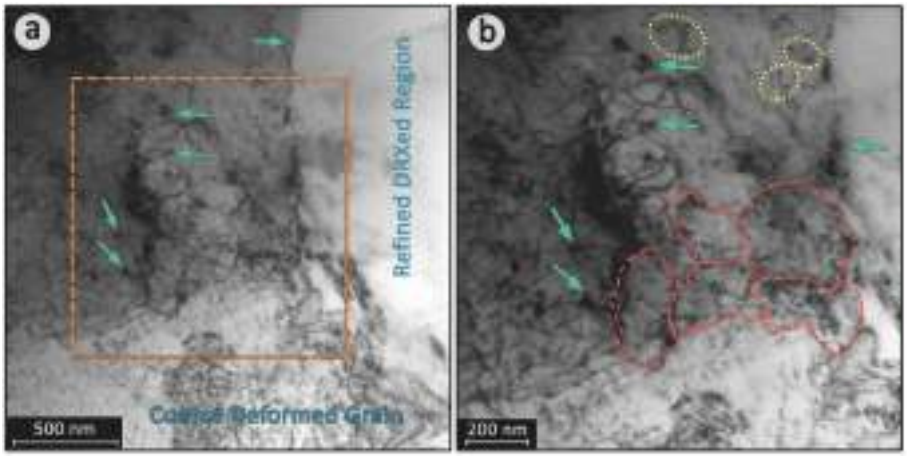

Fig. 7. (a) TEM bright-field image highlighting the microstructural features at the interface between the DRXed region and a coarse deformed grain. (b) High-magnification image.

under hydrogen-rich environments.

3.2.3. TEM characterization

Fig. 7a presents a TEM bright-field image of the processed alloy confirming and expanding upon the observations made via optical microscopy (Fig. 6d). Closer examination validated the formation of fine intermetallic precipitates (highlighted with green arrows) and a remarkable grain refinement achieved through hybrid hot deformation processing, i.e., upsetting and ring rolling. These well-dispersed precipitates, only a few nanometers in size, are located both within the grain interiors and along grain boundaries, as observed in the optical microscopy. This supports the hypothesis of dynamic precipitation occurring during the thermomechanical processing stages, including upsetting and ring rolling, which aligns with the XRD findings [31]. It is widely recognized that the addition of microalloying elements, such as Zn, Ca, and Mn, to Mg alloys promotes dynamic precipitation. Among

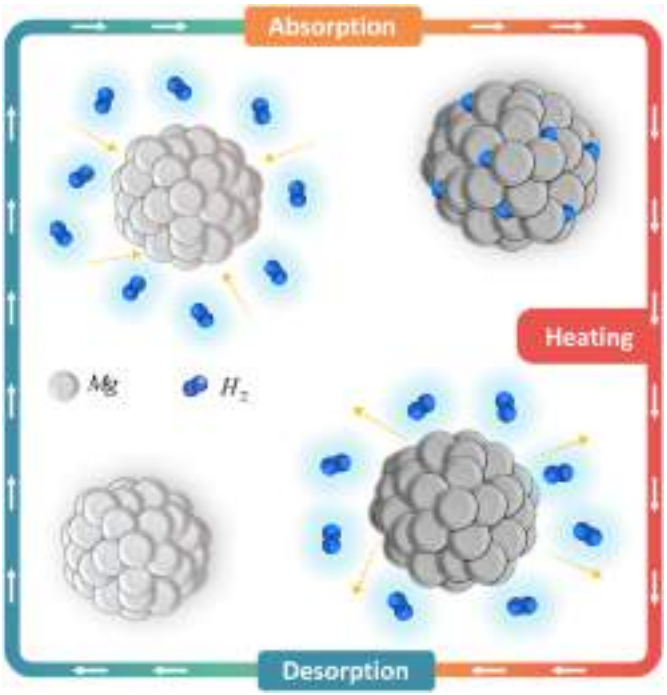

Fig. 8. The hydrogen sorption schematic of Mg hydrogen storages.

these, Ca and Zn are prone to forming Ca–Zn clusters due to the significantly negative enthalpy of mixing between Ca and Zn, which is lower than that of Mg–Zn or Mg-Ca [35]. This segregation creates an energetically favorable condition for the nucleation of dynamic precipitates during deformation [28,36].

Of the box in (a) depicting dislocation tangles, precipitates (green arrows), dislocation substructures (red dashed lines) and Orowan loops (yellow dashed ovals).

These precipitates enhance hydrogen absorption and desorption kinetics by reducing the activation energy required for hydrogen uptake and release. Additionally, they contribute to the structural stability of the alloy during hot deformation, directly influencing its final mechanical properties [10].

Grain refinement is another key factor enhancing the alloy's hydrogen storage properties. The reduction in average grain size increases the density of grain boundaries, which act as energetically favorable sites for hydrogen absorption. Moreover, these grain boundaries facilitate the nucleation of hydride phases [31].

The high density of dislocations, as observed in the TEM image, provides additional diffusion pathways, further accelerating hydrogen transport kinetics. This dislocation density also contributes to the formation of dislocation substructures (indicated by red dashed lines in Fig. 7b) during severe plastic deformation. Recent studies [37,38] confirm that dislocation networks not only facilitate hydrogen diffusion but also reduce diffusion barriers, thereby enhancing absorption and desorption kinetics. Additionally, the presence of dislocation substructures stabilizes the hydride phases and promotes uniform hydrogen distribution during repeated absorption and desorption cycles [10].

Notably, the presence of fine second phases triggers dislocation multiplication (illustrated by Orowan looping in dashed ovals). The resulting increase in dislocation density, in turn, further enhances dynamic precipitation [39].

Another noteworthy feature in Fig. 7 is the heterogeneous microstructure characterized by both recrystallized regions and coarsely deformed grains, plays a critical role in enhancing the alloy's hydrogen storage capabilities. This structure not only provides energetically favorable sites for hydrogen absorption but also facilitates improved hydrogen transport kinetics.

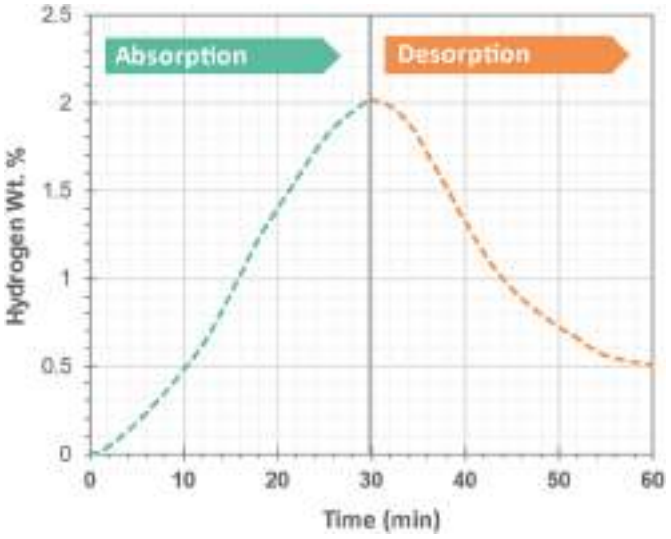

Fig. 9. Hydrogen storage performance of a conventional undeformed Mg alloy.

The combined effects of grain refinement, dislocation substructures, and precipitates create a synergistic relationship between thermomechanical processing and microstructural optimization, significantly improving the alloy's hydrogen storage properties. Moreover, this heterogeneous microstructure effectively reduces the kinetic barriers that typically hinder reversible hydrogen storage, thereby enhancing the efficiency and durability of the material in practical applications.

3.3. Hydrogen sorption behavior

The reaction between magnesium and hydrogen consists of several distinct steps. During hydrogen absorption, the process involves physisorption, dissociation of hydrogen molecules, chemisorption, and diffusion into subsurface and bulk lattice sites, ended with hydride formation through nucleation and growth. For desorption, magnesium hydride decomposes, and hydrogen atoms diffuse to the surface, recombine into hydrogen molecules, and physically desorb (Fig. 8).

The hydrogen absorption and desorption rates in magnesium-based hydrides are controlled by the slowest step in the reaction sequence. This rate-limiting step can be identified using sorption kinetics modeling [39]. Enhancing sorption kinetics can be achieved through several strategies. One critical factor is the microstructure. Grain boundaries, characterized by lower atomic packing density, facilitate faster diffusion than the lattice and serve as favorable nucleation sites for hydride formation and decomposition [40]. Moreover, recent studies [37,38] have demonstrated that a high dislocation density creates additional fast diffusion pathways, modulate local strain fields, and alter hydrogen binding energies, effectively reducing the diffusion barrier. First-principles calculations have further shown that microstructural defects like dislocations and grain boundaries enhance hydriding/dehydriding kinetics by modifying the local electronic structure [41]. The in-situ formed precipitates such as $CaMg_2$ catalyze H_2 dissociation at interfaces through destabilizing MgH_2 and lowering the hydriding enthalpy [42]. These microstructural features synergistically enhance hydrogen absorption and desorption kinetics.

Another key parameter is the material's outer dimension, analogous to particle size in powdered materials. Smaller dimensions increase the surface area available for surface reactions and reduce the diffusion path length for hydrogen within the material. Finally, the addition of suitable catalysts or additives significantly improves sorption kinetics. These catalysts can act as nucleation sites, influence grain and particle size, and catalyze surface reactions.

To optimize absorption kinetics, it is crucial to minimize the hydrogen diffusion path length, which can be achieved by reducing both

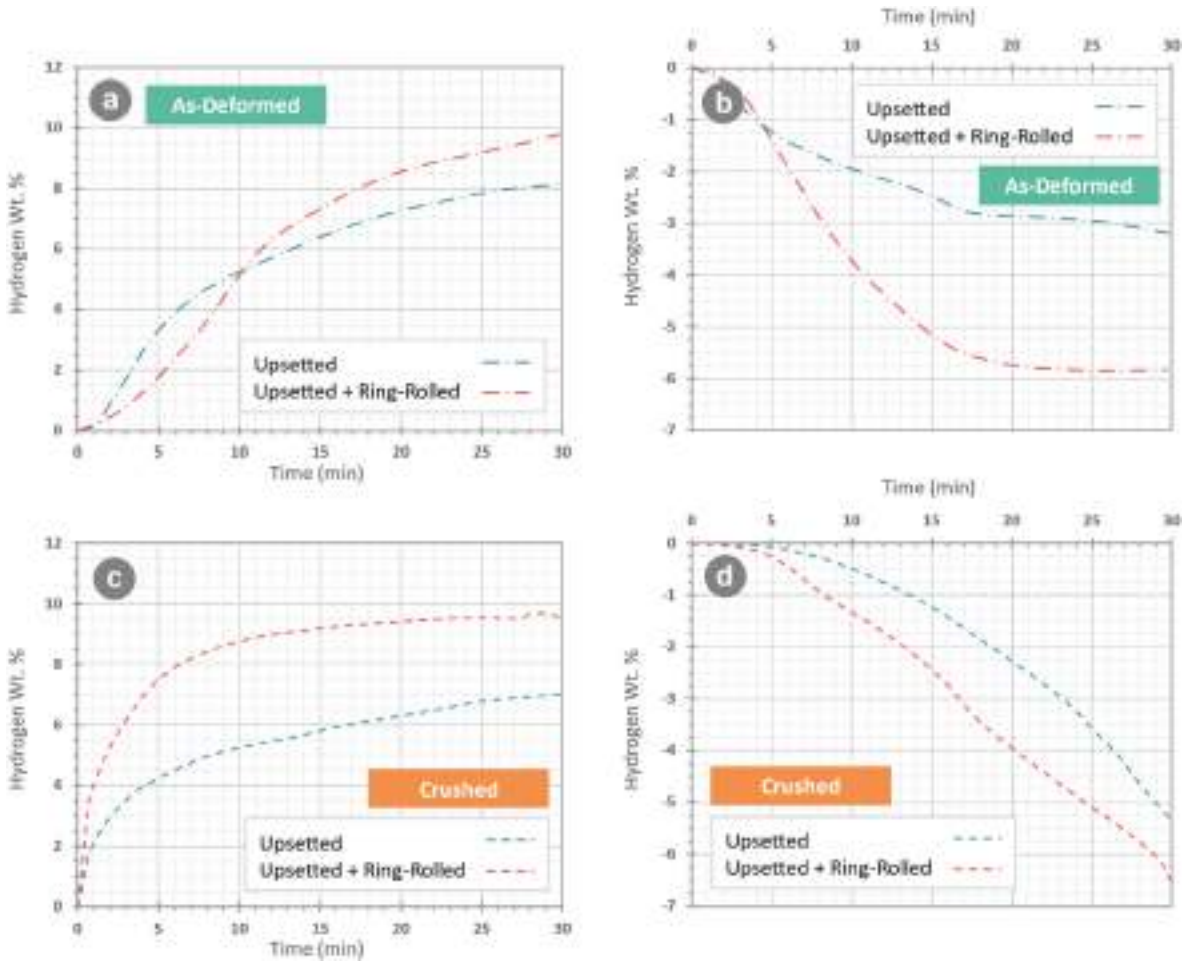

Fig. 10. Kinetic curves showing the initial hydrogen (a) absorption and (b) desorption behaviors of the upsetted and ring-rolled samples. The blue dash-dot curve corresponds to the sole upsetting process, while the red curve represents the upsetted and ring-rolled samples. Panels (c) and (d), respectively, depict the corresponding hydrogen absorption and desorption curves after the samples were crushed. (For interpretation of the references to colour in this figure legend, the reader is referred to the Web version of this article.)

grain and particle sizes [43]. According to Barkhordarian et al. [39], desorption kinetics are primarily limited by surface reactions. Therefore, increasing the surface area (e.g., through smaller particle sizes) and using catalysts can enhance desorption performance. In this study, all controlling factors, including grain size, particle size, and the presence of catalysts, are assessed to comprehensively evaluate the sorption behavior of the modified ZX31 alloy.

3.3.1. *Effect of thermomechanical process*

To evaluate the effect of thermomechanical processing on hydrogen storage performance, the hydrogen absorption and desorption kinetics of the undeformed (original) sample were measured and compared with those of the upsetted and ring-rolled samples. Fig. 9 shows the kinetic curves for the undeformed sample, which exhibits a hydrogen absorption capacity of 0.2 wt% and 0 wt% within 30 min and desorption temperatures of 300 °C and 400 °C, respectively. These values are significantly lower than those of the upsetted and hybrid-processed samples, highlighting the critical role of thermomechanical processing in enhancing hydrogen storage performance [44].

Fig. 10a illustrates the kinetic curves for the initial hydrogen absorption (activation curve) of the upsetted and ring-rolled samples. The absorption tests were conducted at room temperature (25 °C), while the desorption tests were performed at a constant temperature of 325 °C. This desorption temperature is notably lower than the typical temperatures reported for similar Mg-based alloys, which is attributed to the addition of Mn to the alloy composition. Mn acts as a catalytic agent, significantly reducing the desorption temperature. At higher concentrations, Mn has been reported to further reduce the hydrogen desorption temperature, reaching values as low as 250 °C, as reported in a prior study [45].

Conducting hydrogen absorption and desorption experiments at a constant temperature provides a controlled environment to directly compare the kinetics of these processes in the alloy. However, incorporating variable temperature tests in future studies would offer a more comprehensive understanding of the thermodynamic properties and help optimize the hydrogen storage performance of the alloy.

In the sole upsetting process, represented by the red dash-dot curve, the maximum hydrogen absorption reaches 8 wt% within 30 min. The ring-rolled sample, shown by the blue dashed curve, achieves a slightly higher absorption level within the same timeframe. Interestingly, the ZX31 alloy samples processed solely through upsetting demonstrate higher absorption performance compared to other proposed hydrogen storage materials, such as ZK60 processed via equal-channel angular pressing (ECAP) and accumulative roll-bonding (ARB) [46], as well as the AZ91 alloy [11].

It is worth mentioning that a slight delay in hydrogen absorption is observed in the hybrid processed (upsetted + ring-rolled) samples, hindering sorption kinetics during the first 10 min. This delay is likely due to the higher surface area of the ring-rolled sample, which promotes rapid oxidation, forming a magnesium oxide (MgO) layer that obstructs hydrogen penetration. Although the increased strain from the ring-rolling process refines grain size and creates more crystallographic

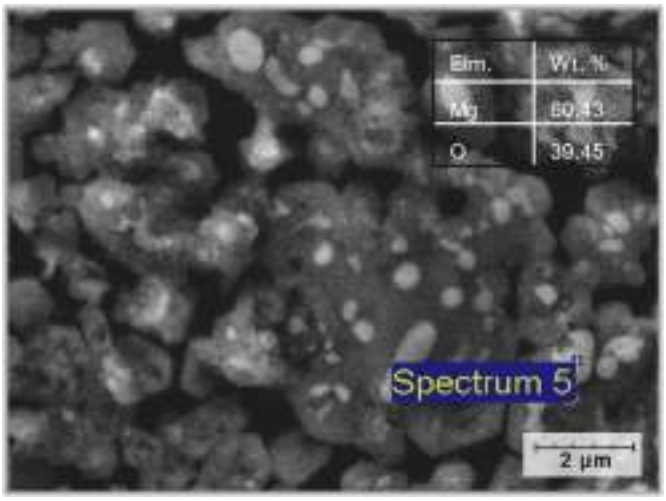

Fig. 11. SEM micrograph of the ring-rolled sample surface. The detected Mg and O (inset table) at the marked location suggest the presence of magnesium oxide (MgO).

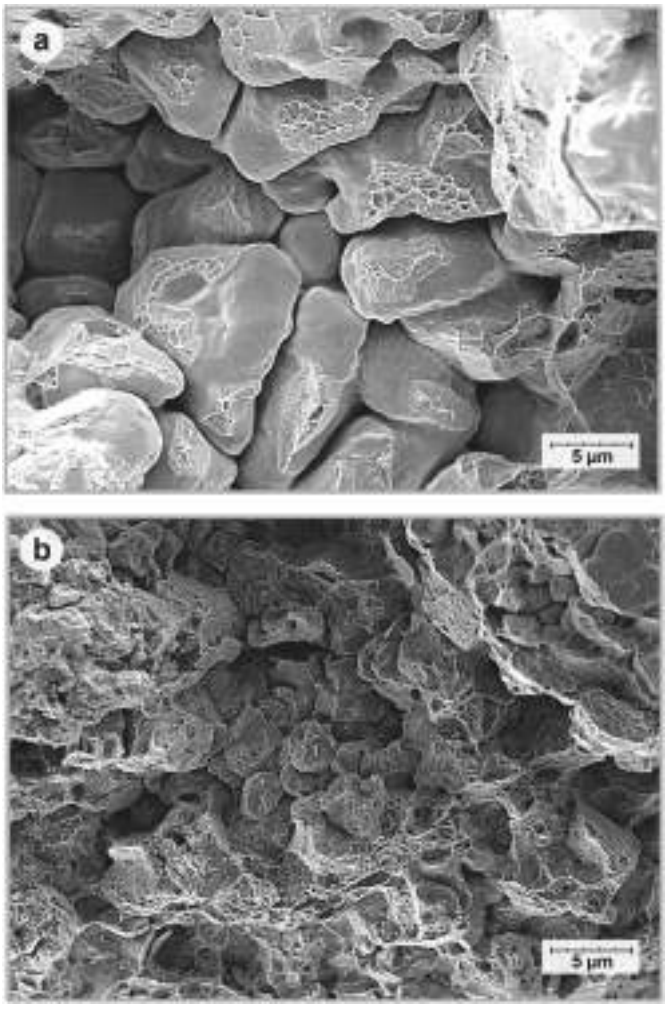

Fig. 12. SEM micrographs of crushed samples processed by (a) upsetting and (b) upsetting followed by ring rolling.

defects—both favorable for hydrogen absorption—the MgO layer on the surface must first be disrupted. In the ring-rolled sample, this disruption process took approximately 10 min, after which the fine-grained inner structure enhanced hydrogen absorption.

Although ring-rolling processing improves hydrogen absorption overall, the hydrogen capacity remains below the maximum absorption potential during the first 15 min. This limitation can be attributed to the samples' morphology, particularly the low surface-to-volume ratio. To address this drawback, the upsetted + ring-rolled samples were crushed into smaller pieces.

To evaluate the influence of the surface oxide layer on hydrogen absorption, energy-dispersive X-ray spectroscopy (EDS) was performed on the ring-rolled sample surface (Fig. 11). The analysis confirmed the presence of a surface oxide layer, with 61 wt% magnesium (Mg) and 39 wt% oxygen (O).

Fig. 11 shows that the oxide layer is distributed uniformly across the surface, with localized regions of higher oxygen concentration. These oxide layers will act as a barrier to hydrogen permeation during the initial stages of absorption, explaining the lower absorption rate observed in the ring-rolled sample during the first 10 min (Fig. 10a). Once the oxide layer is disrupted, either through mechanical cracking or chemical reduction during hydrogen exposure, the underlying microstructure (e.g., grain boundaries, dislocations, and intermetallic phases) becomes accessible, leading to enhanced hydrogen absorption kinetics.

These findings highlight the critical role of surface conditions in controlling hydrogen absorption behavior and provide direct evidence of the oxide layer's influence on the initial absorption kinetics.

3.3.2. *Effect of crushing*

While microstructural refinement improved the sorption behavior of the alloy, further enhancement in hydrogen storage capacity and transfer kinetics can be achieved by increasing the exposed surface area. To this end, the deformed alloy was subsequently crushed into smaller particles.

Fig. 12 shows SEM micrographs of the crushed samples following (a) the upsetting process and (b) the upsetting combined with ring-rolling process. The particle surfaces in both samples predominantly exhibit ruptures along grain boundaries. These ruptures primarily occur in newly recrystallized grains, which formed alongside the original high-angle grain boundaries. A critical feature influencing the absorption capacity of the crushed samples is the roughness of the ruptured surfaces, which enhances the material's exposure to the hydrogen atmosphere and significantly improves hydrogen sorption behavior.

Kinetic curves of the post-crushed hydrogen absorption and desorption behaviors of the upsetted and ring-rolled samples are presented in Fig. 10c and d, respectively. Here, the blue curve corresponds to the sample processed through the sole upsetting process, while the red one represents the upsetted + ring-rolled sample. The absorption curve reaches its maximum potential after approximately 15 min of hydrogen exposure. However, the maximum hydrogen release within a 30-min timeframe is measured at 3 wt%, which is considerably lower compared to prior studies on AZ31 and ZK60 alloys [11,46].

The desorption curves of the crushed sample exhibit a declining trend without reaching a plateau within the first 30 min. This behavior contrasts with that of the non-crushed sample, which plateaus after approximately 20 min, indicating near-complete desorption. The continued decline in the crushed sample's desorption curve suggests that extending the desorption time could enable the alloy to release significantly more hydrogen than measured within the 30-min timeframe. While the current data do not include extended desorption measurements, the observed trend highlights the potential for further hydrogen release beyond the studied duration, consistent with findings in prior studies [39,46]. Future work will focus on extending the desorption time to fully characterize the total hydrogen release capacity of the crushed samples.

The results (Fig. 10a and b) demonstrate the potential of the "upsetted + ring-rolled" sample as a promising option for hydrogen storage applications. This hybrid-processed sample, when further crushed (Fig. 10c and d), displays improved hydrogen sorption kinetics

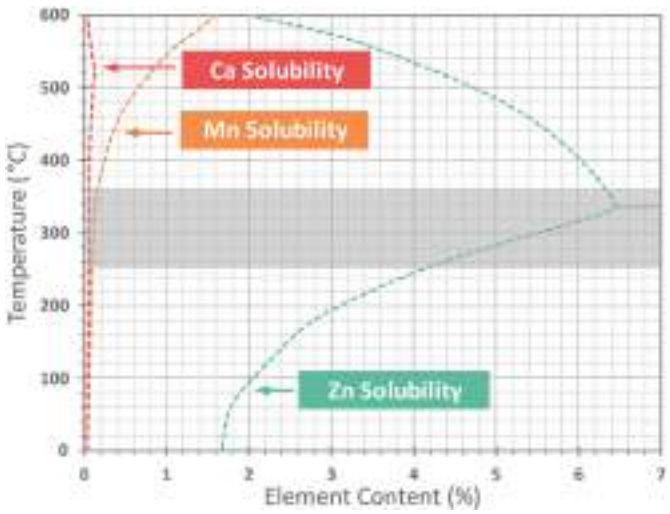

Fig. 13. Alloying elements solubility into the Mg matrix of ZX31 material.

and capacity, primarily due to the enhanced surface roughness and reduced grain size resulting from the combined processing methods.

Overall, the crushed particle morphology plays a significant role in improving hydrogen absorption by increasing the material's exposure to the hydrogen atmosphere. The hybrid processing method enhances this effect, making the upsetted + ring-rolled sample a competitive candidate for advanced hydrogen storage applications.

It is worth mentioning the development of a kinetic model for this SPD-processed alloy is complicated by its multiphase microstructure and defect-rich architecture. Heterogeneous reaction pathways, arising from competing processes such as H_2 dissociation at catalytic interfaces and hydrogen diffusion through phase-segregated precipitates, invalidate simple kinetic models [47]. Furthermore, localized pressure gradients within the DRXed microstructure may dynamically change rate-limiting mechanisms [48]. These complexities highlight the need for hybrid models integrating phase-specific diffusion barriers and defect-driven nucleation terms, which will be explored in future work.

3.3.3. *Effect of alloying elements*

Thermomechanical processing is an effective method to enhance the hydrogen sorption performance of magnesium-based alloys. Beyond this, alloying magnesium (Mg) with selected elements presents an additional strategy to improve its hydrogen storage properties. Incorporating alloying elements that do not form hydrides can significantly influence the stability of the hydride MgH_2 phase. By substituting magnesium with elements that form less stable hydrides, the overall enthalpy of the hydriding reaction is reduced, enabling hydrogen to be released at lower temperatures [49,50].

Furthermore, alloying can introduce new high-energy diffusion pathways that facilitate the movement of hydrogen atoms within the material. These pathways enhance hydrogen transport to inner regions, improving both the kinetics and capacity of hydrogen sorption. This dual benefit of reduced desorption temperatures and accelerated hydrogen diffusion underscores the critical role of alloying in advancing the performance of magnesium alloys for hydrogen storage applications.

For the ZX31 alloy, the synergistic coexistence of $CaMg_2$ and MgH_2 phases plays a crucial role in enhancing hydrogen storage capacity and kinetics. The $CaMg_2$ phase destabilizes MgH_2, effectively lowering the enthalpy of the hydrating reaction, which facilitates hydrogen release at lower temperatures. Moreover, $CaMg_2$ acts as a catalyst by accelerating hydrogen absorption and desorption rates through the creation of additional diffusion pathways for hydrogen atoms [37]. The formation of $CaMg_2$ also contributes to the refinement of the alloy's microstructure, increasing the available surface area for hydrogen absorption while reducing diffusion distances for hydrogen atoms [38]. This refined microstructure not only improves the hydrogenation kinetics but also enhances the material's overall efficiency. Furthermore, $CaMg_2$ supports the structural integrity of the alloy during repeated hydrogenation and dehydrogenation cycles, significantly improving cycling stability and extending the material's lifespan [37]. These combined advantages underscore the potential of alloying magnesium with calcium as an effective strategy for optimizing hydrogen storage performance, making ZX31 a promising material for advanced hydrogen storage applications.

Another effective strategy for destabilizing magnesium hydride (MgH_2) systems, as incorporated in the current alloy, is the formation of an Mg-based solid solution [49]. This method significantly enhances the hydrogen sorption performance of the ZX31 alloy. According to the Mg–Zn binary phase diagram (Fig. 13), zinc exhibits high solubility in magnesium, starting at 3 wt% at room temperature and increasing to 6.2 wt% at 340 °C [39]. This solid solution strategy involves introducing minor modifications to the structure and composition of magnesium, which adjusts its thermodynamic stability while maintaining its hydrogen storage capacity.

This approach is particularly advantageous because it improves the kinetics of hydrogen absorption and desorption, addressing one of the key challenges associated with Mg/MgH_2 systems [50]. The XRD pattern of the processed samples shows several weak peaks corresponding to the $Mg_{0.971}Zn_{0.029}$ solid solution. The formation of this solid solution contributes to the enhanced hydrogen sorption kinetics observed in both bulk and crushed samples during absorption and desorption. Additionally, the activation of mechanisms associated with the solid solution further improves the sorption behavior, making this strategy a valuable tool for optimizing the hydrogen storage performance of the ZX31 alloy. FactSage version 7.2 was used in this study which is an integrated thermodynamic database of chemical thermodynamics. After performing a variety of thermochemical calculations and for the studied phase diagrams and chemical equilibria for these multiphase systems, the solubility of different solutes in Mg matrix was calculated (Fig. 13).

The inclusion of Mn in the Mg–3Zn–1Ca-0.5Mn alloy is motivated by its role as a transition metal (TM) additive, which is well-documented to enhance hydrogen sorption behavior in Mg-based systems [51]. Transition metals, including Mn, form intermetallic phases with Mg (e.g., Mg_3Mn) during alloy preparation. These phases act as catalytic sites that lower the activation energy for hydrogen dissociation and recombination, thereby accelerating absorption/desorption kinetics [1,2]. While binary Mg-TM alloys (e.g., Mg_2Ni, Mg_2Fe) exhibit reduced hydrogen storage capacity compared to pure MgH_2 (7.6 wt% theoretical), their improved thermodynamic and kinetic properties make them indispensable for practical applications [3].

Mn, in particular, contributes to the destabilization of MgH_2 by introducing lattice strain and defects, which lowers the enthalpy of hydrogen desorption. This effect is synergistic with Zn and Ca, which independently refine the microstructure and inhibit oxide formation. For instance, Knotek and Vojtěch [14] demonstrated that ternary Mg–Ni-TM alloys (TM = Mn, Co, Cu, etc.) exhibit enhanced hydrogen diffusion rates due to the catalytic activity of TM additives. In their work, Mn-containing alloys showed improved hydriding/dehydriding kinetics even in as-cast states, emphasizing the importance of TM additives in overcoming kinetic limitations.

Furthermore, Mn improves cyclic stability by mitigating particle agglomeration during repeated hydrogenation cycles, a common issue in pure Mg systems. Its low solubility in Mg promotes the formation of secondary phases at grain boundaries, which serve as hydrogen diffusion pathways. This mechanism aligns with our observations of reduced desorption temperatures and faster kinetics in the Mn-modified alloy. Thus, the addition of Mn complements the roles of Zn and Ca, collectively optimizing the alloy's hydrogen storage performance.

In addition to the $CaMg_2$ phase, the $Ca_2Mg_6Zn_3$ phase plays a critical role in the microstructure and hydrogen storage performance of the ZX31 alloy. During solidification, $Ca_2Mg_6Zn_3$ forms first and acts as a

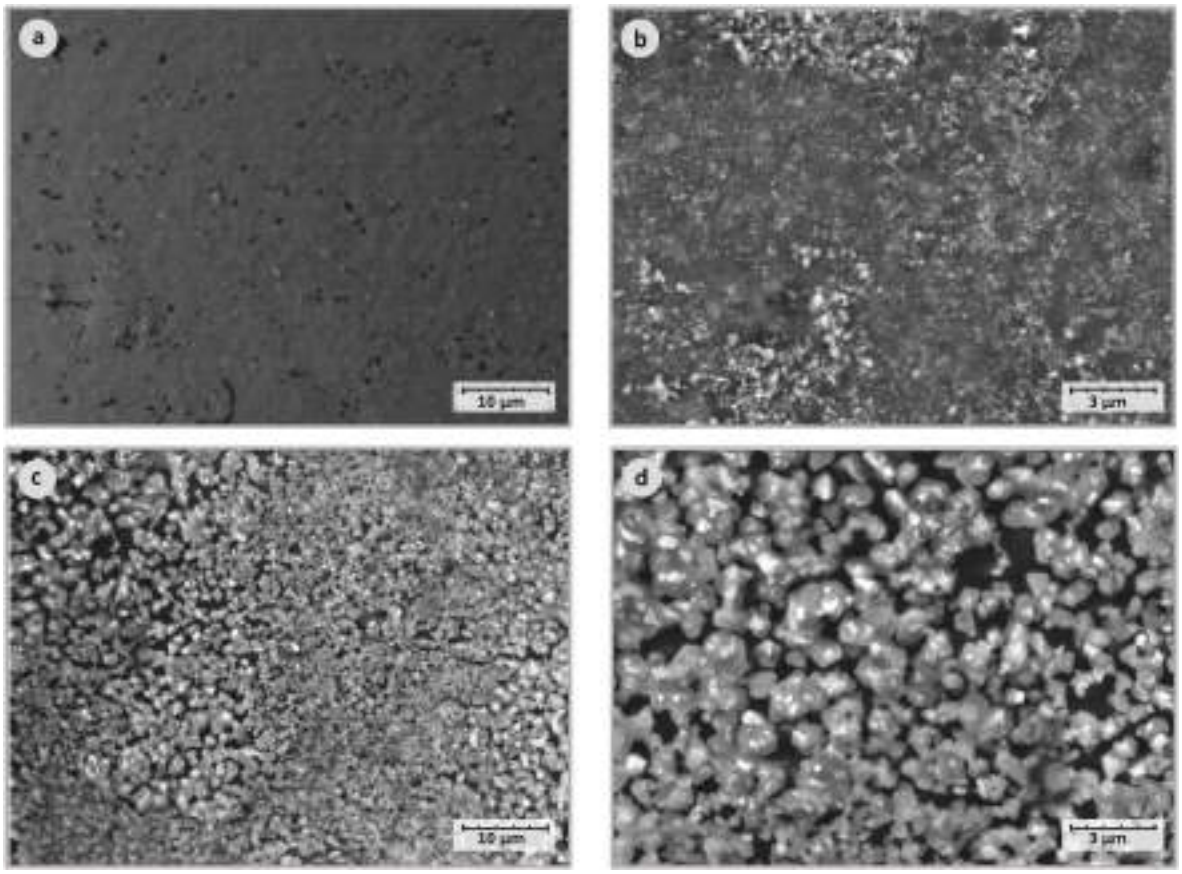

Fig. 14. SEM images of the surface morphology of the Mg–3Zn–1Ca-0.5Mn alloy during hydrogenation; (a) before immersion, (b) after 5 min immersion, (c) after 30 min immersion, (d) the magnified image of (c).

grain refiner by inhibiting excessive dendritic growth, resulting in a finer as-cast microstructure [52]. This refined structure enhances the effectiveness of subsequent thermomechanical processing, such as hot upsetting and ring rolling, in achieving an even finer grain size [53].

During hot deformation, the brittle $Ca_2Mg_6Zn_3$ and $CaMg_2$ phases, which segregate at grain boundaries, fracture and become preferential sites for dynamic recrystallization (DRX). This ensures that these phases are distributed not only at grain boundaries but also within the grain interiors. When the alloy undergoes hydrogen absorption/desorption cycles, the surfaces of the grains that are in direct contact with the hydrogen atmosphere develop microcracks after dehydrogenation [52]. These microcracks enhance hydrogen absorption in subsequent cycles by increasing the surface area and providing additional pathways for hydrogen diffusion.

Furthermore, the presence of $Ca_2Mg_6Zn_3$ throughout the microstructure (as confirmed by SEM images in Fig. 14) ensures that the entire structure, rather than just the grain boundaries, participates in hydrogen absorption and desorption. This phase, along with $CaMg_2$, weakens the covalent bonding between hydrogen and magnesium atoms, thereby reducing the desorption temperature and improving the overall hydrogen storage performance [53].

The synergistic effect of these phases highlights the importance of microstructural control in optimizing the hydrogen storage properties of Mg-based alloys. Future work will focus on further investigating the role of microcracks and phase distribution in enhancing hydrogen absorption/desorption kinetics.

4. Summary and conclusions

A commercial ZX31 magnesium alloy, enhanced with 0.5 wt% Mn, was subjected to thermomechanical processing via industrial scale upsetting and ring rolling to investigate its hydrogen storage behavior.

1. The hydrogen sorption performance of the alloy improved significantly as a result of the processing. Specifically, upsetting and upsetting combined with ring-rolling increased the hydrogen absorption capacity to 8 wt% and 10 wt% within 30 min, respectively.
2. Both the sole upsetting and the hybrid upsetting + ring-rolling processes noticeably enhanced the hydrogen desorption behavior. The hybrid-processed alloy was able to release 6 wt% of its hydrogen content within 20 min.
3. Further processing, such as crushing, if applied, can enhance the hydrogen absorption kinetics in both the solely upset and hybrid-processed samples, providing an additional boost to the sorption performance.

CRediT authorship contribution statement

H. Vafaeenezhad: Supervision, Formal analysis, Data curation, Conceptualization. **B. Nateq:** Visualization, Validation, Resources. **M. Mahmoudi:** Visualization, Validation, Funding acquisition. **M. Fesahat:** Writing – review & editing, Validation, Data curation. **Sh Azizpour:** Visualization, Methodology.

Declaration of competing interest

The authors declare that they have no known competing financial interests or personal relationships that could have appeared to influence the work reported in this paper.

Acknowledgements

The authors would sincerely thank Sajad Moatar for his invaluable contributions to the XRD data analysis.

References

[1] Danaie M, Mauer C, Mitlin D, Huot J. Hydrogen storage in bulk Mg-Ti and Mg-stainless steel multilayer composites synthesized via accumulative roll-bonding (ARB). Int J Hydrogen Energy 2011;36:3022–36. https://doi.org/10.1016/j.ijhydene.2010.12.006.

[2] Tran XQ, McDonald SD, Gu Q, Tan XF, Nogita K. Effect of trace Na additions on the hydriding kinetics of hypo-eutectic Mg–Ni alloys. Int J Hydrogen Energy 2017;42:6851–61. https://doi.org/10.1016/j.ijhydene.2016.12.007.

[3] Silva EP, Leiva DR, Floriano R, Oliveira VB, Pinto HC, Botta WJ. Hydrogen storage properties of filings of the ZK60 alloy modified with 2.5 wt% mischmetal. Int J Hydrogen Energy 2020;45:5375–83. https://doi.org/10.1016/j.ijhydene.2019.05.207.

[4] Castro FJ, Bobet J-L, Urretavizcaya G. Reprocessing different Mg-alloy wastes for hydrogen production by hydrolysis. Int J Hydrogen Energy 2025;99:808–18. https://doi.org/10.1016/j.ijhydene.2024.12.182.

[5] Teichmann N, Hamm M, Pundt A. Fast lateral hydrogen diffusion in magnesium-hydride films on sapphire substrates studied by electrochemical hydrogenography. Int J Hydrogen Energy 2018;43:1634–42. https://doi.org/10.1016/j.ijhydene.2017.11.101.

[6] Sakintuna B, Lamaridarkrim F, Hirscher M. Metal hydride materials for solid hydrogen storage: a review. Int J Hydrogen Energy 2007;32:1121–40. https://doi.org/10.1016/j.ijhydene.2006.11.022.

[7] Nivedhitha KS, Venkatesh R, Banapurmath NR, Ramesh K, Sajjan AM, Subramanian K. Enhancing hydrogen storage capacity: MWCNT-infused Mg–Ti alloy synthesized via mechanical alloying. Int J Hydrogen Energy 2024;67:351–60. https://doi.org/10.1016/j.ijhydene.2024.04.135.

[8] Révész Á, Kis-Tóth Á, Varga LK, Schafler E, Bakonyi I, Spassov T. Hydrogen storage of melt-spun amorphous Mg65Ni20Cu5Y10 alloy deformed by high-pressure torsion. Int J Hydrogen Energy 2012;37:5769–76. https://doi.org/10.1016/j.ijhydene.2011.12.160.

[9] Liu H, Xu L, Han Y, Chen X, Sheng P, Wang S, et al. Development of a gaseous and solid-state hybrid system for stationary hydrogen energy storage. Green Energy Environ 2021;6:528–37. https://doi.org/10.1016/j.gee.2020.06.006.

[10] Asselli AACAC, Leiva DRR, Huot J, Kawasaki M, Langdon TGG, Botta WJJ. Effects of equal-channel angular pressing and accumulative roll-bonding on hydrogen storage properties of a commercial ZK60 magnesium alloy. Int J Hydrogen Energy 2015;40:16971–6. https://doi.org/10.1016/j.ijhydene.2015.05.149.

[11] Floriano R, Leiva DR, Melo GC, Ishikawa TT, Huot J, Kaufman M, et al. Low temperature rolling of AZ91 alloy for hydrogen storage. Int J Hydrogen Energy 2017;42:29394–405. https://doi.org/10.1016/j.ijhydene.2017.10.035.

[12] Huot J, Amira S, Lang J, Skryabina N, Fruchart D. Improvement of hydrogen storage properties of magnesium alloys by cold rolling and forging. IOP Conf Ser Mater Sci Eng 2014;63:012114. https://doi.org/10.1088/1757-899X/63/1/012114.

[13] Wu S, Chen Y, Cai X. Effects of in-situ formed Mg2Ni and Mg2Cu phases on hydrogen storage properties of Mg@Cu9Al4 composite. Int J Hydrogen Energy 2025;103:491–500. https://doi.org/10.1016/j.ijhydene.2025.01.261.

[14] Chen Y, Zheng D, Zhou L, Cai X. Activated carbon-loaded nano-transition metal Ni catalysts for enhancing hydrogen storage behavior of Mg. Int J Hydrogen Energy 2024;95:888–900. https://doi.org/10.1016/j.ijhydene.2024.11.180.

[15] Aguiar VB, Júnior WO, Gonzalez Cruz ED, Leiva DR, Pereira da Silva E. Casting of Mg-based alloy with Ni and Mishmetal addition (Mg88Ni8MM4) for hydrogen storage. Int J Hydrogen Energy 2025;109:63–6. https://doi.org/10.1016/j.ijhydene.2025.02.097.

[16] Deng Y, Chen X, Qi H, Feng S, Wang W, Xie L, et al. The design of Mg–Ti–V–Nb–Cr lightweight high entropy alloys for hydrogen storage. Int J Hydrogen Energy 2024;87:1327–37. https://doi.org/10.1016/j.ijhydene.2024.09.115.

[17] Hu S, Ding X, Chen R, Ma X, Cao W, Shen H, et al. An approach for advancing the hydrogen storage properties via H-induced precipitation of even nanocatalytsts in rapid solidified Mg–Ni–Y alloy fibers. Int J Hydrogen Energy 2024;87:100–6. https://doi.org/10.1016/j.ijhydene.2024.09.043.

[18] Gorbel B, Flamina A, Pathak A, Gupta A, Kumar N. Phase evolution and kinetics investigation of Mg-CaNix composite for hydrogen storage applications. Int J Hydrogen Energy 2025;98:732–40. https://doi.org/10.1016/j.ijhydene.2024.12.111.

[19] Li L, Yang H, Guo L, Sun Z. A control method of guide rolls in 3D-FE simulation of ring rolling. J Mater Process Technol 2008;205:99–110. https://doi.org/10.1016/j.jmatprotec.2007.11.084.

[20] Guo J, Qian D, Deng J. Grain refinement limit during hot radial ring rolling of as-cast GCr15 steel. J Mater Process Technol 2016;231:151–61. https://doi.org/10.1016/j.jmatprotec.2015.12.018.

[21] Wang C, Geijselaers HJM, Omerspahic E, Recina V, van den Boogaard AH. Influence of ring growth rate on damage development in hot ring rolling. J Mater Process Technol 2016;227:268–80. https://doi.org/10.1016/j.jmatprotec.2015.08.017.

[22] Allwood JM, Tekkaya AE, Stanistreet TF. The development of ring rolling technology. Steel Res Int 2005;76:111–20. https://doi.org/10.1002/srin.200505981.

[23] Hua L, Deng J, Qian D. Recent development of ring rolling theory and technique. Int J Mater Prod Technol 2017;54:65. https://doi.org/10.1504/IJMPT.2017.080566.

[24] Davey K, Ward MJ. A practical method for finite element ring rolling simulation using the ALE flow formulation. Int J Mech Sci 2002;44:165–90. https://doi.org/10.1016/S0020-7403(01)00080-7.

[25] Yeom JT, Kim JH, Park NK, Choi SS, Lee CS. Ring-rolling design for a large-scale ring product of Ti–6Al–4V alloy. J Mater Process Technol 2007;187–188:747–51. https://doi.org/10.1016/j.jmatprotec.2006.11.042.

[26] Kil T-D, Lee J-M, Moon Y-H. Quantitative formability estimation of ring rolling process by using deformation processing map. J Mater Process Technol 2015;220:224–30. https://doi.org/10.1016/j.jmatprotec.2015.01.006.

[27] Yao Y, Liu C, Gao Y, Jiang S. Deformation mechanism of Mg-Gd-Y-Zr alloy during hot ring rolling. Mater Char 2021;177:111154. https://doi.org/10.1016/j.matchar.2021.111154.

[28] Yu S, Liu C, Gao Y, Jiang S, Yao Y. Microstructure, texture and mechanical properties of Mg-Gd-Y-Zr alloy annular forging processed by hot ring rolling. Mater Sci Eng 2017;689:40–7. https://doi.org/10.1016/j.msea.2017.02.036.

[29] Luo X, Li L, Xu W, Zhu Y. Effect of driver roll rotational speed on hot ring rolling of AZ31 magnesium alloy. J Magnesium Alloys 2014;2:154–8. https://doi.org/10.1016/j.jma.2014.05.003.

[30] Yea Y, Ko Y, Kim N, Lee J. Prediction of spread, pressure distribution and roll force in ring rolling process using rigid–plastic finite element method. J Mater Process Technol 2003;140:478–86. https://doi.org/10.1016/S0924-0136(03)00721-0.

[31] Nayak S, Kumar Singh A, Gokhale H, Prasad MJNV, Narasimhan K. Optimization of Ti-6Al-4V ring rolling process by FE simulation using RSM. Int J Solid Struct 2023;262–263:112064. https://doi.org/10.1016/j.ijsolstr.2022.112064.

[32] Xie C, Dong X, Li S, Huang S. Rigid–viscoplastic dynamic explicit FEA of the ring rolling process. Int J Mach Tool Manufact 2000;40:81–93. https://doi.org/10.1016/S0890-6955(99)00043-7.

[33] Nayak S, Singh AK, Prasad MJNV, Narasimhan K. Development of microstructural heterogeneities and dynamic restoration activity during ring rolling of Ti-6Al-4V alloy and its tensile response. J Alloys Compd 2023;963:171241. https://doi.org/10.1016/j.jallcom.2023.171241.

[34] Du YZ, Qiao XG, Zheng MY, Wang DB, Wu K, Golovin IS. Effect of microalloying with Ca on the microstructure and mechanical properties of Mg-6 mass%Zn alloys. Mater Des 2016;98:285–93. https://doi.org/10.1016/j.matdes.2016.03.025.

[35] Čapek J, Stráská J, Clausen B, Máthis K. Twinning evolution as a function of loading direction in magnesium. Acta Phys Pol 2015;128:762–5. https://doi.org/10.12693/APhysPolA.128.762.

[36] Schäublin RE, Becker M, Cihova M, Gerstl SSA, Deiana D, Hébert C, et al. Precipitation in lean Mg–Zn–Ca alloys. Acta Mater 2022;239:118223. https://doi.org/10.1016/j.actamat.2022.118223.

[37] Ha H, Jung SJ, Jeong SG, Kim RE, Park H-K, Kim HS. Enhancing hydrogen storage kinetics and capacity via particle size modulation in TiZrCrFeMnNi high-entropy alloy. Int J Hydrogen Energy 2025;99:1047–54. https://doi.org/10.1016/j.ijhydene.2024.12.185.

[38] Wang W, Wang Q, Su H, Zhang L, Guo Y, Lu H, et al. Enhanced cycling durability of A5B19-type single-phase La–Mg–Ni-based hydrogen storage alloy via turning the superlattice structure by Mg. Int J Hydrogen Energy 2024;71:741–9. https://doi.org/10.1016/j.ijhydene.2024.05.120.

[39] Du Y, Du W, Zhang D, Ge Y, Jiang B. Enhancing mechanical properties of an Mg–Zn–Ca alloy via extrusion. Mater Sci Technol 2021;37:624–31. https://doi.org/10.1080/02670836.2021.1938861.

[40] Zhang Y-N, Kevorkov D, Li J, Essadiqi E, Medraj M. Determination of the solubility range and crystal structure of the Mg-rich ternary compound in the Ca–Mg–Zn system. Intermetallics 2010;18:2404–11. https://doi.org/10.1016/j.intermet.2010.08.033.

[41] Pozzo M, Alfè D, Amieiro-Fonseca A, French S, Pratt A. Hydrogen dissociation and diffusion on Ni and Ti -doped Mg(0001) surfaces. J Chem Phys 2008;128:094703. https://doi.org/10.1063/1.2835541.

[42] Lyu J, Lider A, Kudiiarov V. Using ball milling for modification of the hydrogenation/dehydrogenation process in magnesium-based hydrogen storage materials: an overview. Metals 2019;9. https://doi.org/10.3390/met9070768.

[43] Ma Y, Wang D, Li H, Yuan F, Yang C, Zhang J. Microstructure, mechanical and corrosion properties of novel quaternary biodegradable extruded Mg–1Zn–0.2Ca-xAg alloys. Mater Res Express 2020;7:015414. https://doi.org/10.1088/2053-1591/ab6a52.

[44] Zaluska A, Zaluski L, Ström–Olsen JO. Nanocrystalline magnesium for hydrogen storage. J Alloys Compd 1999;288:217–25. https://doi.org/10.1016/S0925-8388(99)00073-0.

[45] Sun Z, Zhang L, Yan N, Zheng J, Bian T, Yang Z, et al. Realizing hydrogen de/absorption under low temperature for MgH2 by doping Mn-based catalysts. Nanomaterials 2020;10. https://doi.org/10.3390/nano10091745.

[46] Zareian Z, Emamy M, Malekan M, Mirzadeh H, Kim WJ, Bahmani A. Tailoring the mechanical properties of Mg–Zn magnesium alloy by calcium addition and hot extrusion process. Mater Sci Eng 2020;774:138929. https://doi.org/10.1016/j.msea.2020.138929.

[47] Zhang J, Li Z, Wu Y, Guo X, Ye J, Yuan B, et al. Recent advances on the thermal destabilization of Mg-based hydrogen storage materials. RSC Adv 2019;9:408–28. https://doi.org/10.1039/C8RA05596C.

[48] Perejón A, Sánchez-Jiménez PE, Criado JM, Pérez-Maqueda LA. Magnesium hydride for energy storage applications: the kinetics of dehydrogenation under different working conditions. J Alloys Compd 2016;681:571–9. https://doi.org/10.1016/j.jallcom.2016.04.191.

[49] Oh-ishi K, Watanabe R, Mendis CL, Hono K. Age-hardening response of Mg–0.3at.%Ca alloys with different Zn contents. Mater Sci Eng 2009;526:177–84. https://doi.org/10.1016/j.msea.2009.07.027.
[50] Ortega Y, Monge MA, Pareja R. The precipitation process in Mg–Ca–(Zn) alloys investigated by positron annihilation spectroscopy. J Alloys Compd 2008;463:62–6. https://doi.org/10.1016/j.jallcom.2007.09.044.
[51] Li B, Peng X, Yang Y, Wei G, Li Q, Chen Y, et al. Enhancement mechanism of low alloying (Mn, Al) and plastic deformation for hydrogen storage kinetics of Mg alloy. Separ Purif Technol 2025;353:128350. https://doi.org/10.1016/j.seppur.2024.128350.
[52] Yin P, Li NF, Lei T, Liu L, Ouyang C. Effects of Ca on microstructure, mechanical and corrosion properties and biocompatibility of Mg–Zn–Ca alloys. J Mater Sci Mater Med 2013;24:1365–73. https://doi.org/10.1007/s10856-013-4856-y.
[53] Li Z, Gu X, Lou S, Zheng Y. The development of binary Mg-Ca alloys for use as biodegradable materials within bone. Biomaterials 2008;29:1329–44. https://doi.org/10.1016/j.biomaterials.2007.12.021.